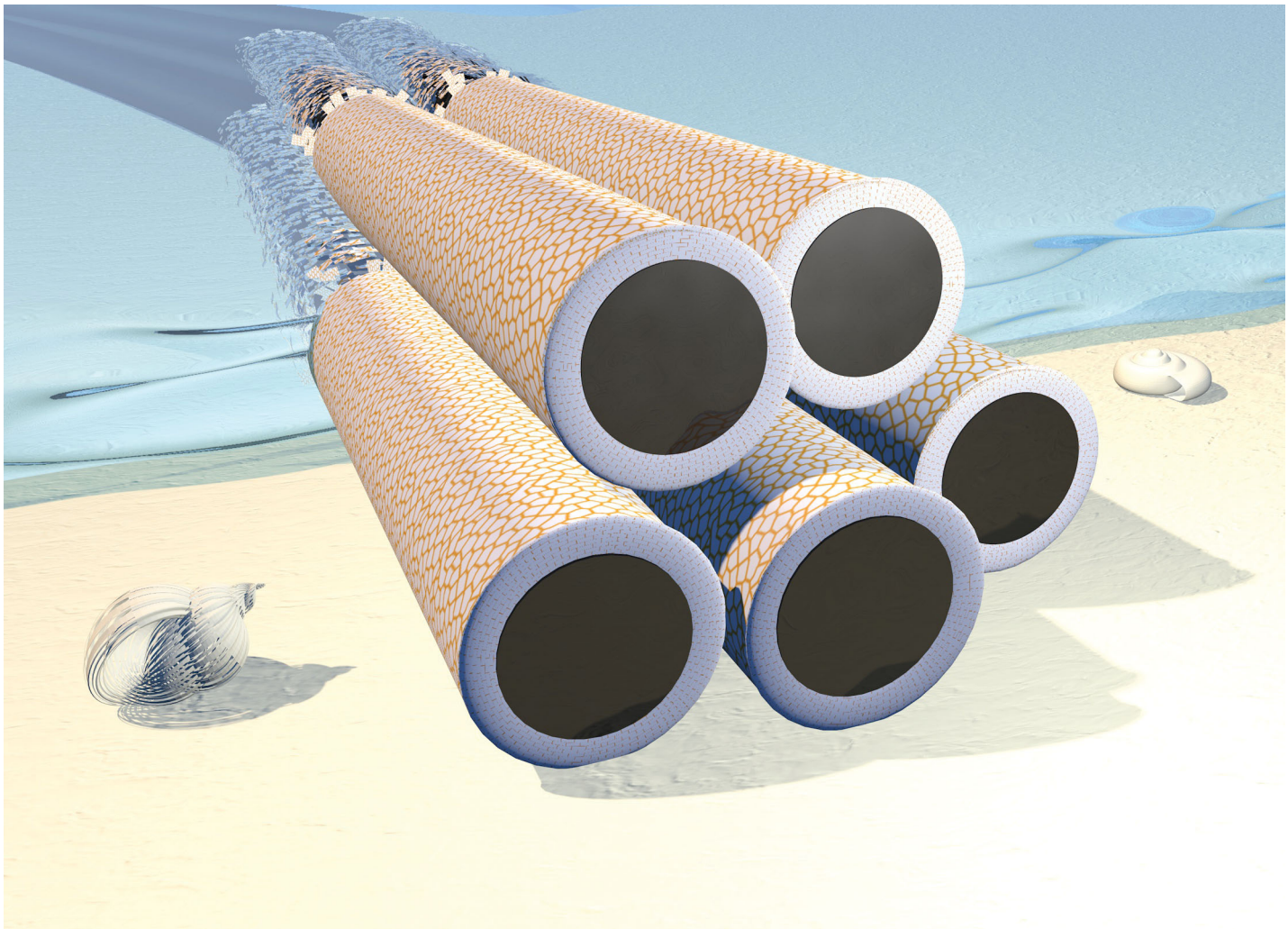

Showcasing a nacre-nanomimetic structure conformally deposited around the circumference of multiple carbon fibres by layer-by-layer assembly by researchers at Imperial College London. Artwork designed and created by Eloise De Luca.

Increasing carbon fiber composite strength with a nanostructured "brick-and-mortar" interphase

Toughening mechanisms occurring in nacre, such as crack deflection and platelet interlocking mechanisms, were reproduced in a nanomimetic coating. The coating was transferred onto the modified surface of carbon fibre tows for use as an interphase. Impregnated fibre tow model composites demonstrated increases in absolute tensile strength and strain-to-failure, as compared to composites containing conventionally sized fibres.

As featured in:

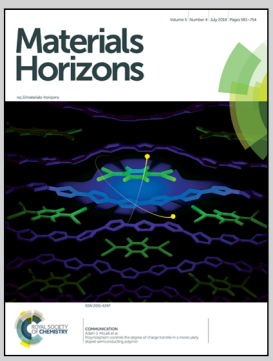

See Milo S. P. Shaffer, Alexander Bismarck *et al.*, *Mater. Horiz.*, 2018, **5**, 668.

ROYAL SOCIETY OF CHEMISTRY

rsc.li/materials-horizons

Registered charity number: 207890

Materials Horizons

COMMUNICATION

View Article Online
View Journal | View Issue

Cite this: *Mater. Horiz.*, 2018, 5, 668

Received 2nd November 2017,
Accepted 21st March 2018

DOI: 10.1039/c7mh00917h

rsc.li/materials-horizons

Increasing carbon fiber composite strength with a nanostructured "brick-and-mortar" interphase†

Francois De Luca,[a] Adam J. Clancy,[bc] Noelia R. Carrero,[bc] David B. Anthony,[a] Hugo G. De Luca,[bc] Milo S. P. Shaffer*[bc] and Alexander Bismarck*[ad]

Conventional fiber-reinforced composites suffer from the formation of critical clusters of correlated fiber breaks, leading to sudden composite failure under tension. To mitigate this problem, an optimized "brick-and-mortar" nanostructured interphase was developed, in order to absorb energy at fiber breaks and alleviate local stress concentrations whilst maintaining effective load transfer. The coating was designed to exploit crack bifurcation and platelet interlocking mechanisms known in natural nacre. However, the architecture was scaled down by an order of magnitude to allow a highly ordered conformal coating to be deposited around conventional structural carbon fibers, whilst retaining the characteristic phase proportions and aspect ratios of the natural system. Drawing on this bioinspiration, a Layer-by-Layer assembly method was used to coat multiple fibers simultaneously, providing an efficient and potentially scalable route for production. Single fiber pull-out and fragmentation tests showed improved interfacial characteristics for energy absorption and plasticity. Impregnated fiber tow model composites demonstrated increases in absolute tensile strength (+15%) and strain-to-failure (+30%), as compared to composites containing conventionally sized fibers.

Conceptual insights

Over the last few decades, the development of conventional fibre-reinforced polymer composites has relied either on tuning the fibre surface chemistry or the matrix composition to optimize fibre/matrix adhesion. Unfortunately, increasing the interfacial strength improves composite strength and stiffness but reduces toughness. We propose a new strategy breaking this established trade off, to create composites with both enhanced tensile properties and toughness by exploiting a well-ordered, nanostructured interphase. The concept is inspired by the properties of natural nacre which combines high strength and toughness. We replicated mechanisms at play in nacre to develop a new composite interphase. The scale and geometry of nacre was scaled down to suit fibre composite systems. A nanostructured coating was deposited by Layer-by-Layer deposition around many carbon fibres, simultaneously, exploiting the self-limiting character of LbL. Large quantities of material can be generated using a simple bath process compatible with continuous fibre processing. The realisation of our nanostructured composite interface results in an increased absolute tensile strength and strain to failure compared to existing state-of-the-art commercial carbon fibre composites. In addition, our concept represents an interesting example of LbL deposition technology, usually time-consuming and limited to small volume deposition.

Introduction

Structural fiber-reinforced polymer (FRP) composites, especially carbon fiber-reinforced composites, are widely used as load-bearing materials due to their high strength and stiffness at low weight. During progressive loading of unidirectional FRPs under tension, fiber breaks occur throughout the whole material, at locations determined by the stochastic fiber strength distribution. When a fiber breaks, the load that it previously carried is transferred to its neighboring fibers through the matrix, generating a local stress concentration. Depending on the geometry, strength distribution and degree of fiber/matrix debonding, the material may be able to redistribute the load successfully, leading to an accumulation of fiber breaks within the composite.[1] Eventually, a critical cluster of fiber breaks forms,[2–4] which is associated with a critical local stress concentration that can no longer be carried by the adjacent fibers, leading to crack propagation and, therefore, sudden and catastrophic failure of the composite.

Composite structures manifest a wide range of toughening mechanisms including interfacial debonding,[5] post-debonding

[a] *Polymer & Composite Engineering (PaCE) Group, Department of Chemical Engineering, Imperial College London, South Kensington Campus, London, SW7 2AZ, UK*
[b] *Department of Materials, Imperial College London, South Kensington Campus, London, SW7 2AZ, UK. E-mail: m.shaffer@imperial.ac.uk*
[c] *Department of Chemistry, Imperial College London, South Kensington Campus, London, SW7 2AZ, UK*
[d] *Polymer & Composite Engineering (PaCE) Group, Institute of Material Chemistry & Research, University of Vienna, Währinger Strasse 42, Wien A-1090, Austria. E-mail: alexander.bismarck@univie.ac.at*

† Electronic supplementary information (ESI) available: Supporting information S1–S7 (Fig. S1–S15), as described in the text. See DOI: 10.1039/c7mh00917h

fiber/matrix friction,[6] fiber pull-out[7,8] and stress relief in the interphase.[9,10] In FRP systems, adhesion at the fiber/matrix interface is often enhanced *via* liquid-phase oxidations,[11] plasma treatments,[12,13] dry gaseous oxidation[14] or electrochemical oxidation,[15] in order to improve the composite strength and stiffness;[16–18] however, toughness is typically reduced. Interleaved architectures have also been investigated as a means to rebalance composite stiffness[19] and toughness.[1] Generally, a weak interface allows for multiple fiber/matrix delaminations and a high degree of energy absorption, at the cost of a reduction in the strength of the composite.[17] A similar dilemma arises when considering the formation of critical clusters of broken fibers. In general, a strong fiber-matrix interface increases the stress concentration in neighboring fibers, encouraging early brittle failure. A weak interface leads to debonding, diffusing the stress concentration, but reducing the integrity of the composite, and increasing the proportion of ineffective fiber length.[1] Fiber coatings, such as polymer interlayers, have been intensively investigated to improve composite toughness by means of interface control.[20,21] Improvements in composite toughness have been reported but at the cost of other mechanical properties. More recently, interlayers containing anisotropic nanoparticles, such as graphene oxide nanosheets, have been explored as a route to increase composite performance through stress redistribution.[22,23] When individualised nanosheets were dispersed in the interphase, increases in the interfacial shear strength (36%) and interlaminar shear strength (13%) were reported, and attributed to redistribution of stresses around the surface crack *via* crack-tip bridging and crack deflection. However, logically, further improvements could be achieved by improving the degree of order of the nanosheets in the interphase; indeed, recent modelling work has shown that a well-defined, layered interphase is needed to improve composite toughness *via* multiple crack deflection.[24] In the context of brittle ceramic matrix composites, where the focus is on toughening, a layered coating of pyrocarbon or boron nitride has been found to be especially effective for crack deflection and stress relaxation, both experimentally[25,26] and numerically.[27] However, for FRPs, simple crack deflection at a weak interface is not sufficient; new approaches are needed to create composite interfaces, which allow composite strength and toughness to be improved simultaneously.[28]

Here, we introduce a nanostructured layered interphase that can be deposited around the circumference of conventional structural carbon fibers. The hypothesis is that an ordered multilayer structure can absorb the energy released by fiber breaks, *via* multiple crack deflections in the layered interphase structure,[29] spreading along the length of the fibers; progressive fiber debonding/slippage, mediated by strain hardening of the interphase layer in shear, can then allow local stress relaxation without excessive debonding. Together, these effects may potentially delay the correlation of fiber breaks in a composite and hence increase its ultimate strength. This concept was inspired by some of the characteristic toughening mechanisms identified in the "brick-and-mortar" structure of natural nacre, such as crack deflection at the platelet interfaces[29] and platelet interlocking[30] in shear. The excellent mechanical performance arising for the well-defined architecture of natural nacre, found in the inner layer of mollusk shells, has recently motivated extensive efforts to produce biomimetic composites with a similar combination of high strength and high toughness.[31] However, typical nacre platelets, both in natural and artificial nacre mimics, are 5 to 10 μm long[32] and cannot be used to produce a coherent layered coating around typical reinforcing fibers, which have diameters of 5 to 15 μm. On the other hand, it is important to retain the critical aspect ratio of the platelets in order to favor the required pull-out and sliding mechanisms.[33,34] The working assumption, based on existing models, is that nacre-like properties can be replicated independently of absolute scale, as long as the aspect ratio of the reinforcing platelets is maintained (at about 10) and the relative thickness of the soft organic layers remains about 5 to 10% of the platelet thickness.[35,36] The thickness of a typical polymer layer, defined by the dimensions of polymer molecules, is around 1–2 nm, and thus platelets should ideally be approximately 10 to 20 nm thick and about 100–200 nm wide. At this scale, the curvature of the fiber is insignificant, and hence a conformal layered structure can, in principle, be accommodated. The range of acceptable platelet dimensions consistent with these requirements is extremely narrow (Supplementary information S1, ESI†). Nevertheless, we were able to design a suitable "brick-and-mortar" nanostructure, consisting of hexagonal layered double hydroxide (LDH) platelets and soft poly(sodium 4-styrene sulfonate) (PSS) polyelectrolyte. We have previously demonstrated the efficacy of this system on flat substrates as well as at the interphase of single glass fiber composites, showing that the correct phase proportions and geometry enabled the mechanical performance and toughening mechanisms of nacre to be reproduced, but at a much smaller length scale.[37,38] Here, we report the deposition of this nanoscaled nacre mimic around structural carbon fibers. Due to its self-limiting nature, the Layer-by-Layer (LbL) method provides a convenient route to generate a well-ordered coating on multiple fibers simultaneously. The effect of a nanostructured composite interphase was quantified on the single fiber level and in model impregnated tow composites.

Results and discussion

The LbL process is based on electrostatic forces, and requires the substrate to have a high surface charge density to allow for successful deposition and adequate adhesion. Commercial industrially oxidized, unsized carbon fibers have only a limited charge density (Fig. 1A and Supporting information S3, ESI†), which leads to weak interactions with the deposited coating (Supplementary information S2, ESI†). Therefore, the carbon fibers were further oxidized by O_2 plasma treatment and subsequent immersion in 0.1 M $KMnO_4$; the resulting (additional) acidic surface oxides dissociate, particularly at high pH, resulting in an increased negative surface charge density (Supporting information S3, ESI†). While the exposure to O_2 plasma did not cause any measurable reduction in carbon fiber diameter,

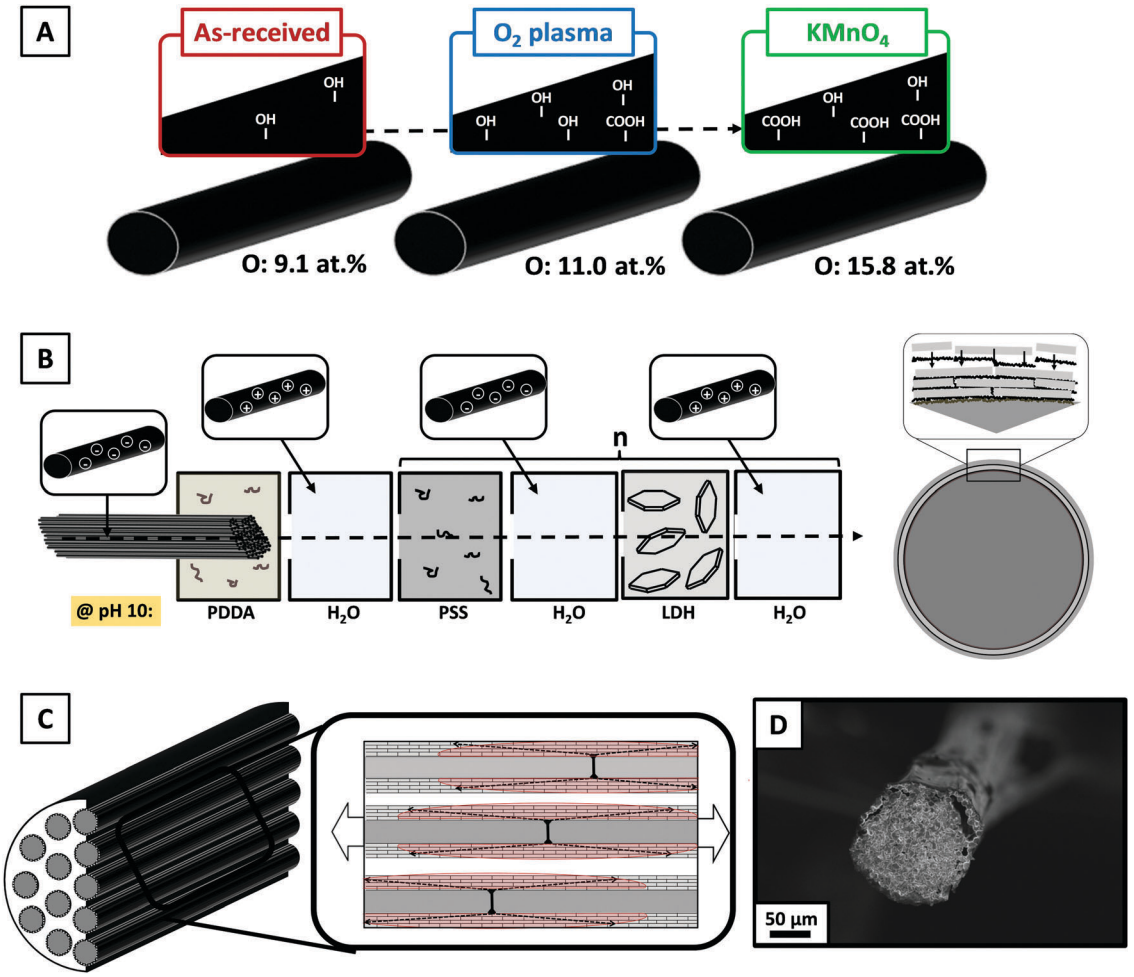

Fig. 1 Schematic diagram showing the modification of the as-received unsized carbon fibers, coating deposition and small composite manufacture: the as-received carbon fiber surfaces were functionalized with low-pressure O_2 plasma treatment and subsequently further oxidized in $KMnO_4$ (A). PDDA(PSS/LDH)$_n$ "brick-and-mortar" nanostructures were assembled, by LbL at pH 10, on all the individual carbon fibers within a bundle (B). The composite containing coated carbon fibers was intended to fail *via* crack deflection (in red) and sliding within the volume of the anisotropic nanostructured interphase (C). SEM micrograph of a composite cross-section made of coated carbon fibers (D).

etching of the surface crenulations was observed, leading to higher surface roughness particularly at longer treatment times (Supporting information S3, ESI†). A short 5 min plasma treatment was used to increase surface charge whilst retaining a low surface roughness needed to form well-ordered, nanostructured LbL deposits. Disordered versions of these "brick-and-mortar" nanostructures on glass substrates are known not to allow for platelet pull-out or effective crack deflection,[37,38] likely limiting improvements in composite tensile properties.

The measured ζ-potentials showed that all fibers were negatively charged over the entire pH range. The initial plateau value around −19 mV, characteristic for industrially oxidized carbon fibers,[39] increased in magnitude after O_2 plasma treatment to −45 mV, and again to −58 mV following $KMnO_4$ treatment, as expected on introducing more dissociable acidic functional groups (Supporting information S3, ESI†).[39,40] In order to improve the electrostatic interactions between the fiber surface and the coating, all the solutions and suspensions used for the LbL deposition were adjusted to pH 10, where the ζ-potential was most negative, similar to the deposition of the coating on glass slides.[37]

Bundles of commercial PAN-based unsized treated carbon fibers (diameter 7 μm) were successfully coated (called "coated fibers" in the following) *via* a sequential LbL dipping process (Fig. 1B). A soft, cationic poly(diallyl dimethyl ammonium chloride) (PDDA) precursor layer was found to promote the adhesion of the coating to the fiber, avoiding direct contact between the stiff, positively-charged platelets and rigid carbon fiber surfaces. The negatively charged fiber surfaces were first coated with a positive PDDA buffer layer, before repeatedly applying (PSS/LDH) bilayers. As found for coatings[37] successfully deposited on both flat substrates and curved surfaces of glass fibers,[38] using the same methodology and constituent materials, the coating thickness increased linearly with the number of deposited (PSS/LDH) bilayers by about 15 nm per bilayer, indicating a stable, ordered LbL process (Supplementary information S4, ESI†). Additional SEM micrographs of coatings deposited on both carbon fibers and flat substrates reveal a

similar morphology (Supporting information S4, ESI†). SEM showed that the PDDA/(PSS/LDH)$_n$ coatings were homogeneous across all the fibers within the bundles. The self-limiting nature of the LbL process means that each individual fiber within the bundle can be coated simultaneously, accelerating production and allowing small unidirectional model composites, consisting of several hundred coated carbon fibers in epoxy to be manufactured (Fig. 1C and D).

In order to assess the effect of the nanostructured interphase on the properties of the fiber/matrix interface in epoxy, single fiber pull-out tests were carried out for both the coated fibers and "control fibers" (plasma and $KMnO_4$ oxidized, unsized carbon fibers). Both the apparent interfacial shear strength (IFSS) and ability of the fiber to progressively slide during the debonding process were investigated (Fig. 2A and B). Stable fiber slippage was quantified by defining the debonding length ratio (DLR) as the ratio between the distance that the fiber slides prior to full debonding (l_d) over the fiber length embedded in epoxy (l_e). The IFSS was determined from a plot of maximum force against embedded area (Fig. 2A); the consistency of the IFSS as a function of the fiber embedded length, within error, indicated a valid ductile failure mode (Fig. 2B).[41] Both IFSS and DLR were significantly improved by the presence of the nanostructured coating, relative to the control fibers, reaching maxima of 59.5 ± 3.9 MPa (+84%) and 0.17 ± 0.02 (+89%), respectively, for the fibers coated with a 0.4 μm thick PDDA/(PSS/LDH)$_{25}$ layer. Further increases in the interphase thickness resulted in a relative drop of the IFSS and DLR, most likely due to a reduction of the radial clamping force exerted on the fiber by the epoxy matrix, as a result of the compliance of the coating.

Single fiber fragmentation tests were conducted on both the control fibers and the optimum PDDA/(PSS/LDH)$_{25}$ coated fibers, to assess the ability of the nanostructured interphase

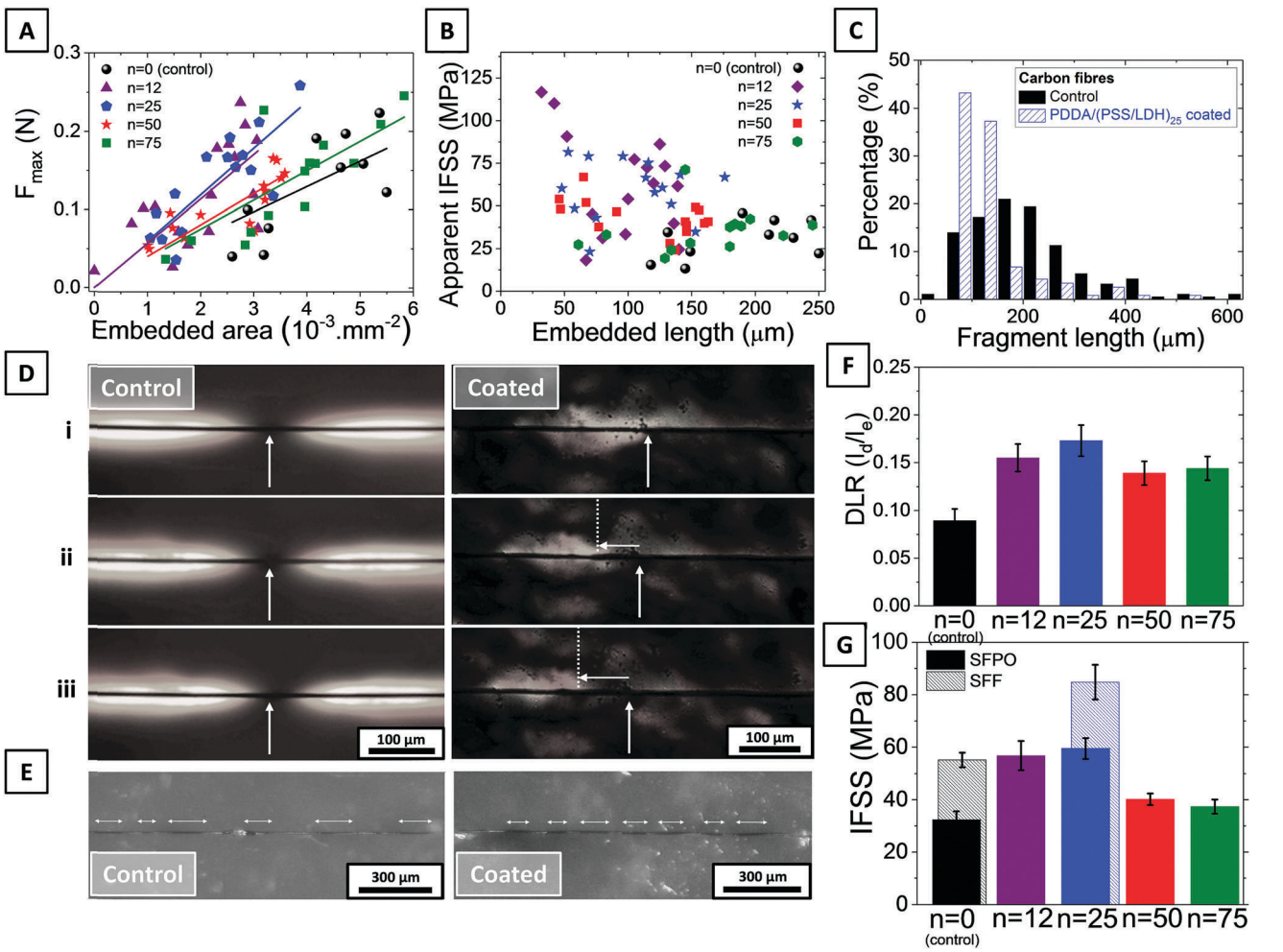

Fig. 2 Maximum force (F_{max}) applied to single fibers as a function of fiber embedded area in the epoxy matrix (A), apparent IFSS = $f(l_e)$ of control fibers and fibers coated with PDDA/(PSS/LDH)$_n$ of varying thickness (B) and histogram distribution of fiber fragment length for control and PDDA/(PSS/LDH)$_{25}$ coated fibers obtained by single fiber fragmentation tests (C). Optical images of *in situ* fragmentation of control and PDDA/(PSS/LDH)$_{25}$ coated (D) carbon fibers using cross-polarized light in transmission at +1.2% and +2.4% strain (i, ii and iii, respectively); vertical arrows pinpoint fiber fragments and horizontal arrows and the dashed line highlight progressive sliding of the fiber. Optical images of control and PDDA/(PSS/LDH)$_{25}$ coated carbon fibers using non-polarized light in transmission mode after the fragmentation test (E); horizontal arrows show fiber fragments. Debonding length ratio (DLR) and IFSS of carbon fibers coated with different PDDA/(PSS/LDH)$_n$ coating thicknesses determined by single fiber tests in epoxy (F and G, respectively).

to redistribute/dissipate stress under more realistic loading conditions. The photoelastic birefringence, observed by polarized transmission optical microscopy during testing, relates to stress concentrations at the fiber/matrix interface in the vicinity of fiber breaks.[42] The control fibers exhibited an intense and large stress field near each fiber break, which remained relatively unchanged when strain increased (Fig. 2D(i–iii)); in contrast, the PDDA/(PSS/LDH)$_{25}$ coated fibers presented a less intense stress field, spread along the length of the fiber (Fig. 2C and D). Upon increasing the macroscopic strain, the stress field was observed to propagate progressively along the fiber, accompanied by a noticeable further reduction in intensity of the stress field. The weaker initial stress field can be attributed to crack deflection within the nanostructured "brick-and-mortar" interphase, while the reduction in its intensity can be attributed to progressive slippage of the fiber, through plastic deformation of the interphase. The fragment length distributions, after saturation, were shifted towards shorter lengths for the coated fibers (Fig. 2C, mean lengths of 212 ± 11 and 137 ± 9 μm for control and coated fibers, respectively). Critical fragment lengths (l_c) of 283 ± 14 and 182 ± 12 μm were deduced from the mean fragment length using the Kelly-Tyson model[8] (refer to Method). Although the strength of the fibers at the scale of the fiber fragments is uncertain, IFSS values were estimated using a tensile strength of 4413 MPa (provided by the manufacturer, Hexcel). IFSS values of 55.2 ± 2.8 and 84.8 ± 6.6 MPa were determined for the control and PDDA/(PSS/LDH)$_{25}$ coated fibers, respectively, showing a significant enhancement in broad agreement with the IFSS increase measured from single fiber pull-out tests (Fig. 2G).

The tensile properties and fracture behavior of small unidirectional model composites were compared against control fibers, and the optimum PDDA/(PSS/LDH)$_{25}$ coated fibers, as well as additional samples prepared with as-received commercially-sized PAN-based fibers (called "sized fibers" in the following). To ensure good impregnation of a bundle of coated fibers and, therefore, achieve a high fiber volume fraction in the composite, the resin must wet the fibers. Flat micrometre-thick nanostructured coatings with LDH- and PSS-terminated monolayers were used in order to identify which interface was best wetted by the liquid, uncured epoxy resin. A similar, favourable contact angle was observed in each case, about 22° and 23° for the LDH- and PSS-terminated coatings, respectively (Supporting information, S6, ESI†). For consistency with the single fiber tests, LDH-terminated coatings were used for the composite bundle experiments. Homogeneous impregnation of the bundles with the ultra-low viscosity epoxy resin led to composites with a fiber volume fraction around 50%, determined from micrographs of cross-sections (Supporting information S6, ESI†). The tensile stress–strain responses of these tow composites were recorded and correlated with acoustic events (AEs), indicative of fiber breaks (Fig. 3A) occurring during the tensile test. In order to minimize any effect of varying fiber volume fractions and, therefore, allow for a fair comparison of the different composite specimens, the load applied to the material was converted into a stress normalized to the cross-sectional area of the

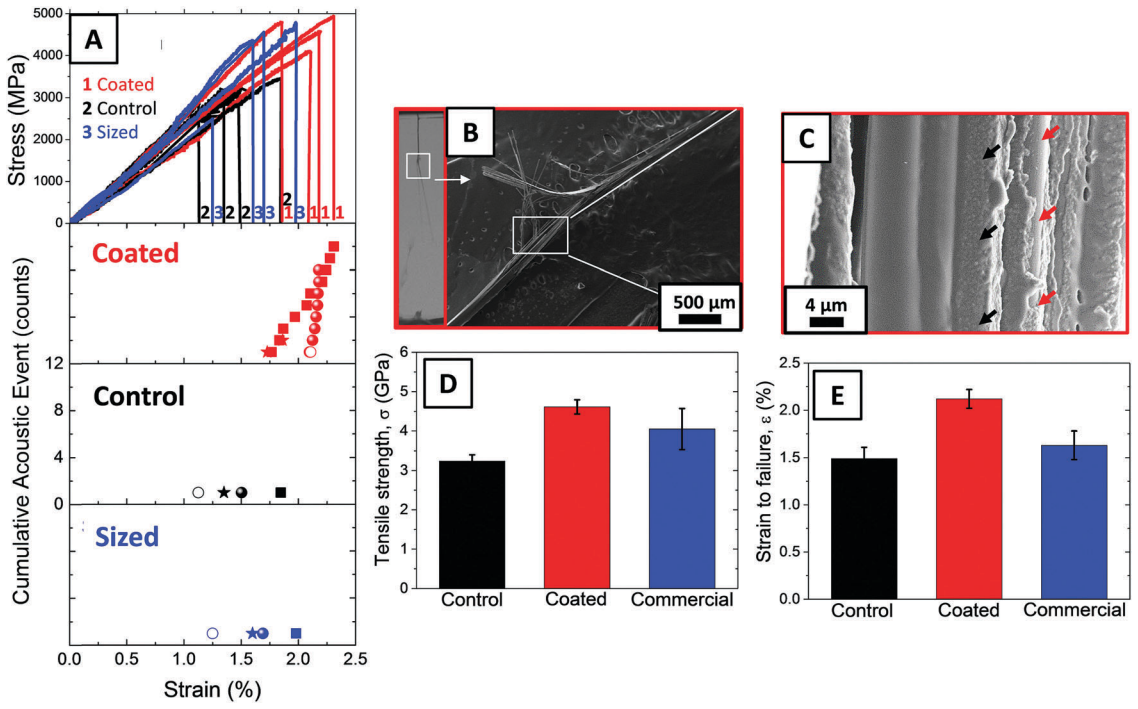

Fig. 3 Stress–strain curves and associated cumulative distributions of acoustic emission events occurring during tensile tests of impregnated fiber tow composites containing control fibers, coated fibers (with "brick-and-mortar" PDDA/(PSS/LDH)$_{25}$ nanostructured coating), and sized fibers (A). Low and high magnification SEM micrographs, accompanied by high speed video stills, of fracture surfaces of impregnated fiber tow composites containing coated fibers (B and C, respectively) – red and white arrows pinpoint locations where the coating is removed and still adhered to the surface of the fibers, respectively. Tensile strength and strain-to-failure of the composites containing control, coated and sized fibers (D and E, respectively).

Table 1 Tensile properties of the different unidirectional bundle composites

Composite specimen	Elastic modulus/GPa	Strength/GPa	Strain-to-failure/%	AE events/a.u
Coated	232.54 ± 3.99	4.61 ± 0.18	2.12 ± 0.10	1–10
Control	218.32 ± 18.50	3.24 ± 0.16	1.49 ± 0.12	Final rupture only
Sized	249.06 ± 15.87	4.05 ± 0.52	1.63 ± 0.15	Final rupture only

total fiber content in the composite. This approach provides a clearer indication of the fiber dominated tensile properties, which determine the tensile properties of unidirectional tow composites. The strain was recorded using a video extensometer across the full gauge length of the specimens. The elastic modulus was determined to be similar for all types of fiber composites, roughly 230 GPa (Table 1); the similarity to the expected elastic modulus of AS4 carbon fibers (231 GPa) confirms the robustness and consistency of the composite preparation and testing. The tensile strength of the tow composites containing the nanostructured interphase increased from 3235 ± 160 MPa to 4607 ± 391 MPa, as compared to composites containing the control fibers (Fig. 3D). The increased tensile strength of the coated fibers was accompanied by an increased strain-to-failure from 1.49 ± 0.12% to 2.12% ± 0.10% (Fig. 3E). More importantly, the strength and strain to failure of the coated fiber composites also exceeded the values for the sized fibers (4048 ± 523 MPa and 1.63 ± 0.15%, respectively). Only a single AE event was detected for the composites based on control or sized fibers, which was associated with the final composite failure. However, for the composites containing coated fibers, additional AE events were detected, prior to failure. This observation is consistent with a larger number of independent fiber breaks occurring in the hierarchical composites, due to a successful reduction in local stress concentrations in neighboring fibers. The associated delay in the formation of a critical cluster of fiber breaks can explain the improved ultimate tensile strength and strain to failure of the composites.

The fracture surfaces of the failed composites were investigated by SEM and showed distinctive differences. The sized fiber composites showed a brittle and localized failure, with no pull-out (Supporting information S7, ESI†). The control fibers show debonding (Supporting information S7, ESI†), with relatively clean fiber surfaces, attributed to poorer fiber/matrix adhesion; the IFSS of the sized fibers was measured to be about 48% higher than that of the control fibers (48.1 ± 1.4 MPa) by single fiber pull-out tests (Supporting information S5, ESI†). In contrast, the coated fiber composites also showed debonding but with a mixture of rough and smooth surfaces, indicating that the coating remained partly attached to the fiber until fracture (Fig. 3B and C). At lower magnification, the fracture surfaces of the coated fiber composites exhibited a more staggered final failure, than the control or sized fiber systems, indicating multiple fracture sites (Supporting information S7, ESI†).

Conclusions

An entirely new class of nanostructured fiber sizing was designed and successfully implemented. Highly ordered nanostructured multilayered nacre mimetics were scaled down by more than an order of magnitude, in order to conformally deposit them around the circumference of conventional structural carbon fibers. A 0.4 μm thick "brick-and-mortar" PDDA/$(PSS/LDH)_{25}$ nanostructured coating was found to offer the greatest improvements in IFSS and DLR, as determined by single fiber pull-out. In fragmentation tests, the local stresses associated with fiber fragmentation appeared reduced and diffused. The findings are consistent with the intended mechanisms of crack deflection and platelet interlocking in shear within the composite interphase, whilst simultaneously improving load transfer between matrix and fibers. When the optimum coating was used as the interphase in unidirectional impregnated fiber tow model composites, the new system provided higher ultimate strength and strain-to-failure than composites containing either bare unsized treated carbon fibers ("control fibers") or the as-received commercially-sized carbon fibers ("sized fibers"). Acoustic emission recorded a higher number of fiber breaks within the hierarchical composites prior to the final catastrophic failure, indicative of the occurrence of multiple isolated fiber breaks. The nanostructured "brick-and-mortar" interphase appears to have isolated fiber breaks within the composite, delaying the formation of a critical cluster, leading to improved tensile properties compared to the composite containing commercial fibers. Further development should allow for additional improvements in strength and strain to failure, particularly by improving the stability of the coating under tension and increasing its adhesion to the fibers *via* covalent bonding. The molecular weight of the polyelectrolyte could be optimized to maintain an ideal bilayer thickness whilst allowing maximum shear strain under load. Ultimately, a more ductile composite response might be observed if a sufficiently high density of isolated fiber breaks could be achieved. One can assume that a thicker PDDA/$(PSS/LDH)_n$ nanostructured interphase ($n > 25$) may allow for more energy dissipation along the length of the fibers, reducing interactions between broken fibers and, therefore, allowing for higher tensile strength, if the radial clamping force can be maintained. The deposition of the coating around many individual fibers within a bundle of fibers offers the possibility to manufacture tows of coated fibers in a continuous manner, *via* a simple sequence of dipping baths, similar to current sizing deposition methods. The scalability of the deposition process on carbon fiber tows might result in a practical use of Layer-by-Layer assembly, since the parallel deposition process increases the volume production rate, whilst a relatively thin coating on each fiber is sufficient to alter the composite properties. This approach offers an appealing method to produce a wide range of complex fiber sizes effectively.

Funding Sources

This work was funded under the UK Engineering and Physical Sciences Research Council (EPSRC) Programme Grant EP/I02946X/1 on High Performance Ductile Composite Technology in collaboration with the University of Bristol. Supporting data are available, subject to a non-disclosure agreement. Please contact the corresponding author in the first instance.

Conflicts of interest

There are no conflicts to declare.

Acknowledgements

We greatly acknowledge Joshua Elsdon for designing and building the robotic dipping LbL system used for this research.

References

1 G. Grail, S. Pimenta, S. T. Pinho and P. Robison, *Compos. Sci. Technol.*, 2015, **106**, 100–109.
2 A. E. Scott, I. Sinclair, S. M. Spearing, A. Thionnet and A. R. Bunsell, *Composites, Part A*, 2012, **43**(9), 1514–1522.
3 D. B. R. Aroush, E. Marie, C. Hauthier, S. Youssef, P. Cloetens and H. D. Wagner, *Compos. Sci. Technol.*, 2006, **66**(10), 1348–1353.
4 A. E. Scott, M. Mavrogordato, P. Wright, I. Sinclair and S. M. Spearing, *Compos. Sci. Technol.*, 2011, **71**(12), 1471.
5 J. D. Outwater and L. C. Murphy, Paper 11C, 24th Annual Technical Conference of Composites, 1969.
6 A. Kelly, *Proc. R. Soc. London, Ser. A*, 1970, **319**(1536), 95–116.
7 J. K. Kim, C. Baillie and Y.-W. Mai, *J. Mater. Sci.*, 1992, **27**(12), 3143–31574.
8 A. Kelly and W. R. Tyson, *J. Mech. Phys. Solids*, 1965, **13**(6), 329–350.
9 G. Marom and R. G. C. Arridge, *Mater. Sci. Eng.*, 1976, **23**, 23–32.
10 V. A. Matonis and N. C. Small, *Polym. Eng. Sci.*, 1969, **9**(2), 90–99.
11 Z. Wu, C. U. Pittman and S. D. Gardner, *Carbon*, 1995, **3**(5), 597–605.
12 A. Bismarck, M. E. Kumru and J. Springer, *J. Colloid Interface Sci.*, 1999, **210**, 60–72.
13 K. K. C. Ho, S. Lamoriniere, G. Kalinka, E. Schulz and A. Bismarck, *J. Colloid Interface Sci.*, 2007, **313**(2), 476–484.
14 A. Bismarck, D. Richter, C. Wuertz and J. Springer, *Colloids Surf., A*, 1999, **159**(2), 341–350.
15 M. R. Alexander and F. R. Jones, *Carbon*, 1995, **33**(5), 569–580.
16 M. Labronici and H. Ishida, *Compos. Interfaces*, 1994, **2**(3), 199–234.
17 J. Karger-Kocsis, H. Mahmood and A. Pegoretti, *Prog. Mater. Sci.*, 2015, **73**, 1–43.
18 M. Sharma, S. Gao, E. Mader, H. Sharma, L. Y. Wei and J. Bijwe, *Compos. Sci. Technol.*, 2014, **102**, 35–50.
19 H. A. Maples, S. Wakefield, P. Robinson and A. Bismarck, *Compos. Sci. Technol.*, 2014, **105**, 134–143.
20 G. C. Papanicolaou, S. A. Paipetis and P. S. Theocaris, *Colloid Polym. Sci.*, 1978, **256**(7), 625–630.
21 J. K. Kim and Y. W. Mai, *Compos. Sci. Technol.*, 1991, **41**(4), 333–378.
22 X. Zhang, X. Fan, C. Yan, H. Li, Y. Zhu, X. Li and L. Yu, *ACS Appl. Mater. Interfaces*, 2012, **4**(3), 1543–1552.
23 W. Qin, F. Vautard, L. T. Drzal and J. Yu, *Composites, Part B*, 2015, **69**, 335–341.
24 G. Dai and L. Mishnaevsky, *Compos. Sci. Technol.*, 2014, **91**, 71–81.
25 R. Naslain, *Compos. Interfaces*, 1993, **1**(3), 253–286.
26 R. Naslain, *Composites, Part A*, 1998, **29**(9–10), 1145–1155.
27 N. Carrère, E. Martin and J. Lamon, *Composites, Part A*, 2000, **31**(11), 1179–1190.
28 H. W. Rhee and J. P. Bell, *Polym. Compos.*, 1991, **12**(4), 213–215.
29 R. Z. Wang, H. B. Wen, F. Z. Cui, H. B. Zhang and H. D. Li, *J. Mater. Sci.*, 1995, **30**, 2299–2304.
30 K. S. Katti, D. R. Katti, S. M. Pradhan and A. Bhosle, *J. Mater. Res.*, 2005, **20**(5), 1097–1100.
31 N. A. Yaraghi and D. Kisailus, *Annu. Rev. Phys. Chem.*, 2017, DOI: 10.1146/annurev-physchem-040215-112621.
32 F. D. Fleischli, M. Dietiker, C. Borgia and R. Spolenak, *Acta Biomater.*, 2008, **4**(6), 1694–1706.
33 S. Pimenta and P. Robinson, *Compos. Sci. Technol.*, 2014, **104**, 111–124.
34 H. D. Espinosa, J. E. Rim, F. Barthelat and M. J. Buehler, *Prog. Mater. Sci.*, 2009, **54**(8), 1059–1100.
35 S. Bekah, R. Rabiei and F. Barthelat, *J. Bionanosci.*, 2011, **1**(1–2), 53–61.
36 F. Barthelat, *J. Mech. Phys. Solids*, 2014, **73**, 22–37.
37 F. De Luca, R. Menzel, J. J. Blaker, J. Birkbeck, A. Bismarck and M. S. P. Shaffer, *ACS Appl. Mater. Interfaces*, 2015, **7**(48), 26783–26791.
38 F. De luca, G. Sernicola, M. S. P. Shaffer and A. Bismarck, *ACS Appl. Mater. Interfaces*, 2018, **10**, 7352–7361.
39 A. B. Garcia, A. Cuesta, M. A. Montes-Moran, A. Martínez-Alonso and J. M. Tascón, *J. Colloid Interface Sci.*, 1997, **192**(2), 363–367.
40 K. Grundke, M. Boerner and H. J. Jacobasch, *Colloids Surf.*, 1991, **58**(1–2), 47–59.
41 S. Meretz, W. Auersh, C. Marotzke, E. Schulz and A. Hampe, *Compos. Sci. Technol.*, 1993, **48**(1–4), 285–290.
42 S. Feih, K. Wonsyld, D. Minzari, P. Westermann and H. Lihol, *Forskningscenter*, 2004.

